Capacitive pressure sensing with suspended graphene-polymer heterostructure membranes – Supplementary Information

Christian Berger,[1] *Rory Phillips,*[1] *Alba Centeno,*[2] *Amaia Zurutuza*[2] *and Aravind Vijayaraghavan*[1]*

[1] School of Materials and National Graphene Institute, University of Manchester, Manchester, M13 9PL, UK.

[2] Graphenea S.A., 20018 Donostia-San Sebastián, Spain.

* Corresponding author email: aravind@manchester.ac.uk

Supplementary Discussion 1: Fabrication of suspended graphene and graphene-polymer heterostructure membranes

Sensor fabrication begins with a graphene flattening process (Figure 1, step 1). A copper foil of 5 mm x 5 mm size with CVD-graphene on its top surface is coated with a thin poly(methyl methacrylate) (PMMA) layer by spin-coating and baking at 130°C for 5 minutes (Figure 1, step 1a). The foil is then floated in a 2.5 wt/vol % aqueous ammonium persulfate solution for 4 hours in order to etch away the copper (Figure 1, step 1b). The remaining graphene-PMMA membrane is then transferred into a deionised (DI) water bath by fishing it with a microscope slide. This process is repeated for two further DI water baths, in 15 minute intervals to allow contaminants to be cleaned from the graphene surface (Figure 1, step 1c). After the third DI water bath the film is transferred onto a plasma cleaned Si/SiO_2 substrate using the same fishing method (Figure 1, step 1b). As the water dries from this substrate the graphene-PMMA stack conforms to the surface of the SiO_2. On baking the dried substrate at 130°C for 15 minutes the PMMA reflows allowing the graphene to further flatten onto the substrate surface. The second step in the sensor fabrication is to release a homogenous graphene-polymer heterostructure from the substrate (Figure 1, step 2). Although the graphene is now relatively flat, the PMMA layer is inhomogeneous and has built in strain as it was initially formed on an undulated copper foil whose surface morphology does not match that of the flat SiO_2 surface. Therefore, the substrate comprising the flattened graphene is first submerged in acetone followed by hexane in order to remove the PMMA layer used in the initial transfer process. Once dried, a new PMMA layer (PMMA 950 3 wt% in anisole) is spin-coated (3000 rpm for 60 s) and baked (130°C for 5 mins). A tape support window that has an opening slightly larger than the target sensor area is then adhered to the substrate (Figure 1, step 2a). The substrate with tape support window is then submerged in an aqueous potassium hydroxide solution (30 wt%) for up to 5 hours until the tape support window and graphene-PMMA membrane lifts off the substrate and floats on the

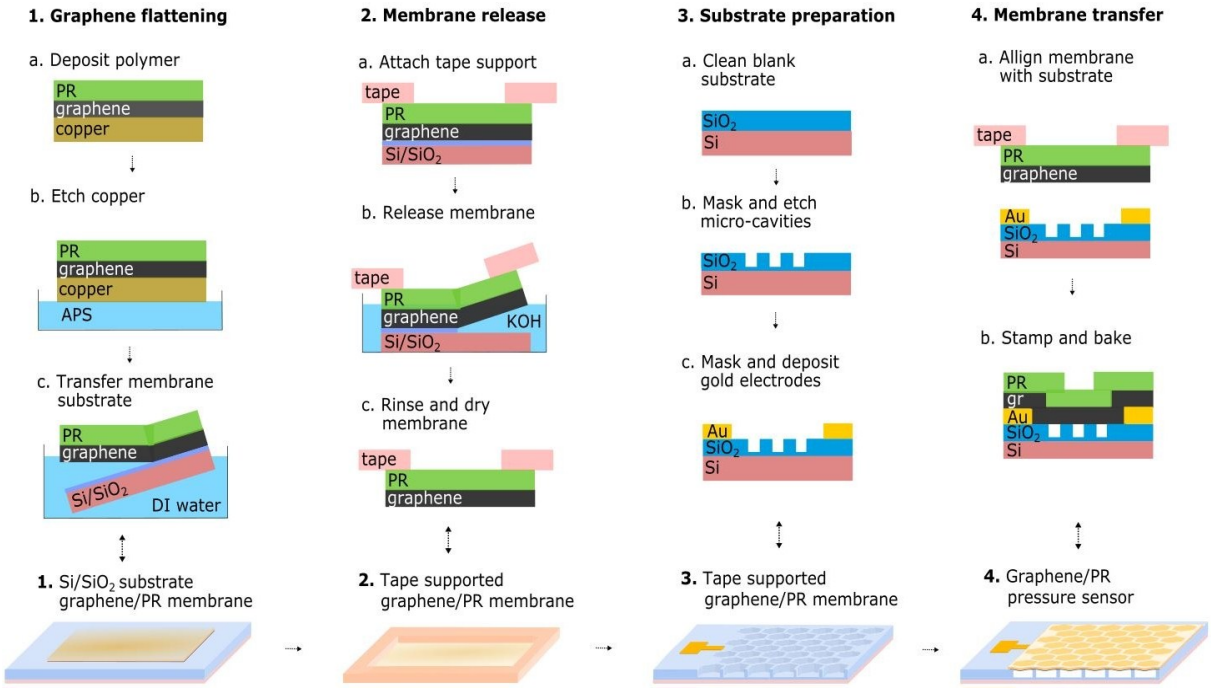

Figure 1 | Fabrication protocol of capacitive graphene-polymer membrane pressure sensor.

solutions surface (Figure 1, step 2b). Similarly to step 1, the tape supported membrane is cleaned in 3 subsequent DI water baths before it is removed from the final bath with tweezers using the tape as a handle (Figure 1, step 2c). The next step is to form the target substrate comprising cavities and electrodes (Figure 1, step 3). On a separate Si/SiO_2 substrate, a positive photoresist mask (Shipley S1813) is exposed using an optical lithography system (Microtech LaserWriter). The substrate is then developed (Shipley MF319) and patterned by deep reactive ion etching using CHF_3 and Ar gas (Oxford Plasma Lab 100) to form an array of circular or hexagonal holes of a given diameter, periodicity and depth, arranged in various patterns such as a hexagonally packed lattice (Figure 1, step 2b). The remaining photoresist is then removed with acetone and another positive photomask is formed using a double layer resist (Shipley PMGI and S1813) to define electrode structures. A thermal evaporator (Moorfield Nanotechnology) is then used to deposit 5 nm chromium followed by 70 nm gold followed by removal of the double layer photoresist using developer (MF319) and acetone (Figure 1, step 3c). In the final step the tape supported graphene-PMMA film is aligned with the target substrate using an in-house built transfer system (Figure 1, step 4a).[1] The graphene-PMMA film is then brought into contact with the substrate and the edges of the film are torn using a sharp tipped tool, releasing the tape window support (Figure 1, step 4b).

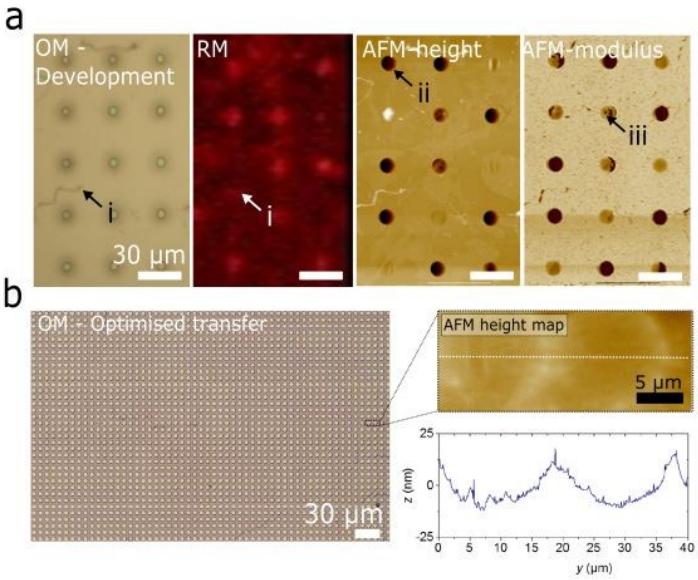

Figure 2 | Characterisation of graphene-polymer capacitive pressure sensor. (**a**) Optical micrograph (OM), Raman Map (RM), Atomic Force Microscope height map (AFM-height) and AFM modulus maps (AFM-modulus) of the same area of a graphene-polymer membrane sample in demonstrating the typical device artefacts encountered in the development; i: Contaminants that appear as suspended membranes, ii: Sagging membranes that appear as collapsed in AFM height maps, iii: Fractured membranes that appear as intact in AFM height maps. (**b**) Optical micrograph and AFM cross-section of optimised graphene-polymer array for comparison. Scale bars = 30 µm for all figures.

Supplementary Discussion 2: Characterisation of suspended graphene-polymer membrane arrays.

In order to optimise the fabrication procedure we employed a series of optical and mechanical techniques that can be used in parallel to identify the failure mechanism of collapsed membranes. Sensors were first imaged by optical microscopy (OM) to check for rips, cracks or contaminants in the graphene-polymer film (Figure 2a, arrow i). Samples with full covera ge and homogenous film transfer were then analysed by Raman spectroscopy and atomic force microscopy (AFM). Renishaw Streamline™ Raman mapping allowed us to map the signiture G (1580 cm^{-1}) and 2D (2680 cm^{-1}) peak intensities over the entire sample area. We found that the G peak intensity gave the highest contrast between suspended and substrate-supported regions due to laser interference effects from the variation in effective refractive index through air in comparison to SiO_2 (Figure 2a, RM). We note that great care must be taken when identifying suspended membranes since contaminants can show an enhanced Raman signal that is easily mistaken for a suspended membrane (arrow i). Further characterisations of successfully transferred films is undertaken by AFM Quantitative Nanomechanical Mapping (QNM).[2] This mode of AFM allows us to create high resolution maps of the height (AFM-height) and effective elastic modulus (AFM-modulus) of our device. The combination of height and modulus data allows us to cross-check if membranes are truly suspended and highlights any cracks or tears (Figure 2a, arrow iii) in the membranes that may not be visible from optical microscopy and Raman mapping. For comparison, an optimised graphene-polymer transfer (Figure 2b) shows a homogenous array of suspended graphene-polymer membranes. The AFM height scan in th right imag of Figure 2b shows that the array of mmbranes consists of evenly suspended membranes that gently sag into the cavities.

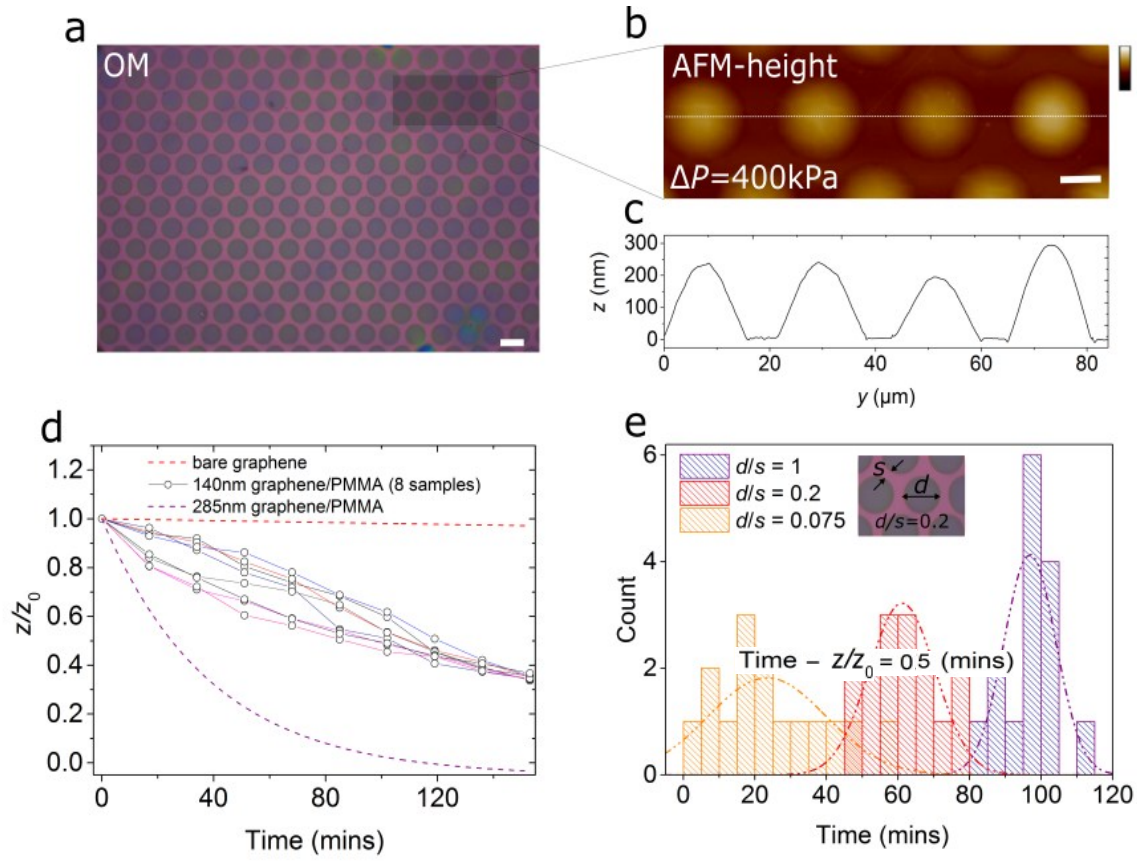

Figure 3| Nitrogen gas leakage from graphene-polymer micro-blisters (**a**) An optical micrograph of a close packed array of 15 µm diameter membranes with a thickness of 140 nm at equilibrium pressure. Scale bar: 20 µm. (**b**) An AFM height map of the magnified area in Figure 2a pumped to 400 kPa resulting in micro-blisters. Scale bar 20 µm. (**c)** A cross-section of the white dotted line in Figure 2b shows the deflection of four micro-blisters inflated to 400 kPa. (**d**) The deflation of micro-blisters from 400 kPa over 157 minutes. Eight samples of each bare graphene, 140 nm and 285 nm graphene-polymer are displayed. Best fit lines of the bare graphene and 285 nm graphene-polymer samples are shown for clarity. (**e**) The time taken for devices of three different cavity densities to deflate to of 0.5.

Supplementary Discussion 3: Characterisation of gas permeability of graphene-polymer membranes

In order to characterise the gas permeability of the graphene-polymer membranes we applied a micro-blister inflation technique. Firstly, pressure sensor samples were inserted into a pressure chamber equipped with a commercial reference pressure sensor and a gate valve, allowing precise control over the chamber pressure. The chamber was pumped with N_2 gas to 400 kPa and left for 24 hours allowing gas to diffuse into the micro-cavities, equilibrating the pressure across the membrane. Samples were then removed from the pressure chamber, causing the membrane to form a blister above the micro-cavity. Samples were then mounted on an AFM within 5 minutes of removing samples from the pressure chamber. We then monitored the maximum point of deflection, z, of the micro-blisters periodically over 3 hours. Figure 3a shows an optical micrograph of a device under test at equilibrium pressure and the AFM height map and cross-section in Figure 3b and c shows the same device immediately after sample removal from the pressure chamber. Figure 2d shows the membrane deflection, z, of 8 individual membranes relative to their maximum deflection, z_0. In the first hour

of deflation we observe an increasing spread in deflections which converges again after approximately 1 hour. This suggests that the reference pressure reading used to conduct pressure sensing measurements would have limited accuracy as the cavities leak gas over time. We repeated this deflation experiment for 8 bare graphene and 285 nm graphene-polymer samples each for comparison and the membrane deflection is plotted over time in Figure 3d. The deflation of bare graphene samples is negligible as expected due to its gas impermeability and ultra-strong adhesion to the micro-cavity edge, providing a gas tight seal.[3,4] The slight decrease in deflection is likely due the porosity of the SiO_2 as previous reports suggest. 285 nm graphene-polymer membranes on the other hand show a rapid decrease in deflection. We attribute this increase in gas leakage due to the increased bending rigidity of thicker membranes, reducing the ability of membranes to fully conform to the substrate and adhere via van der Waals forces. In addition, the use of a large scale transferred film, comprising a continuous CVD graphene sheet ensures minimal gas leakage through the membranes. Instead, we expect the gas pressure in neighbouring micro-cavities to equilibrate via nano-channels along the substrate-membrane interface. To support this hypothesis we fabricated three substrates comprising arrays of cavities of varying density described by the ratio of micro-cavity diameter, d, to its spacing from neighbouring cavities, s. Figure 3e shows the distribution of times taken for 3 samples of varying cavity density with a thickness of 140 nm to deflate to $/z_0 = 0.5$. This demonstrates the correlation between the leakage rate and micro-cavity density, suggesting that high density arrays are mostly limited to dynamic pressure sensing. Moreover, it gives an indication of the timescales over which the measured sensor performance is representative of the model described above. We note that thermal treatment of the polymer-layer temporarily softens the graphene-polymer membrane allowing it to form an improved substrate-graphene interface that can further increase the gas impermeability of the membranes.[5]

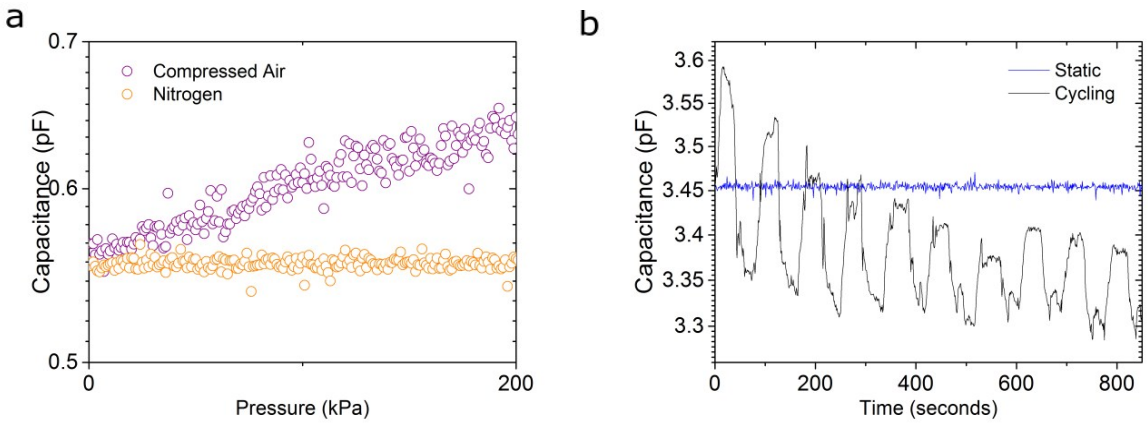

Figure 4 |Calibration of pressure sensing system. (a) Variation of capacitance as a function of pressure of reference devices containing no cavities using compressed air and nitrogen pressurising gases of three consecutive pressure cycles between 0 and 200 kPa. (b) The change in capacitance of a single device when the pressure is cycled between 0 and 100 kPa compared to when the device is kept static.

Supplementary Discussion 4: Pressure sensor calibration

We characterised the effect of surface adsorbates measuring the change in capacitance of a reference device using compressed air and nitrogen gas individually. The reference device comprised a 1 mm^2 graphene-polymer square transferred onto a plain Si/SiO_2 substrate with no cavities. The response of three consecutive pressure cycles between 0 and 200 kPa of the reference device is shown Figure 4a. Whilst compressed air gave a capacitance variation of approximately 0.1 pF over a 200 kPa pressure change, nitrogen gas showed negligible variations. Thus we conducted all pressure cycling experiments in a nitrogen atmosphere. We further investigated the onset of drift in devices by monitoring the capacitance of a cavity-baring device over an extended period of time when cycled between 0 kPa and 100 kPa in comparison to when kept at equilibrium pressure. Figure 4b shows that negligible drift is observed under static loading whilst cycling not only causes gradual decrease in drift during cycling, but also the sensitivity of the sensor before stabilising after some time. We attribute this behaviour to the initial relaxation of fabrication induced stresses which are readily relieved on multiple pressure cycles of the membranes. In order to ensure minimal drift and reproducibility in the sensor performance we cycled all sensors for several minutes before measurement.

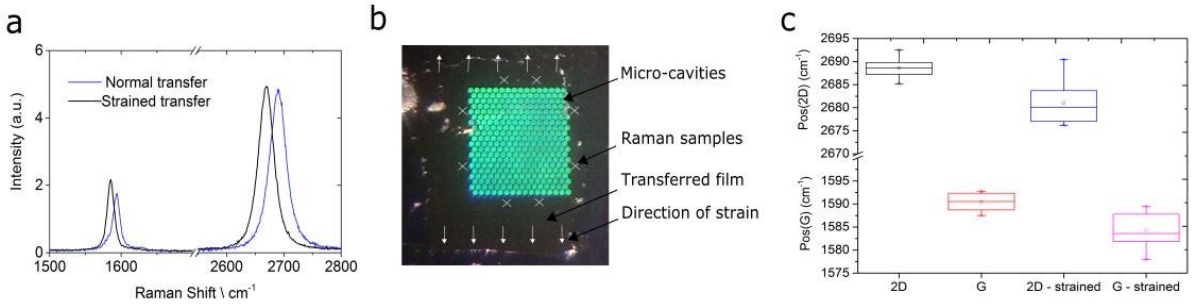

Figure 5 | Strain transfer characterisation. (a) Raman spectrum of an arbitrary reference point on a supported section of two individual graphene-polymer films transferred using the normal and strained transfer techniques. (b) A photograph of a second generation device indicating the direction of strain and 8 sample points at which Raman spectra were taken. Scale bar 100 µm. (c) Chart indicating the spread of peak positions of the signature 2D and G peak of graphene in graphene-polymer films transferred normally and strained.

Supplementary Discussion 5: Raman spectroscopy of strained graphene-polymer films

The Raman spectra of a strained and unstrained sensors with device design 2 were compared (Figure 5a) in order to estimate the applied strain on the graphene. In total, eight sample points spread around the perimeter of the cavity array were probed on each of the two samples as shown in Figure 5b. We ensured each sample point was taken on flat portions of the substrate in order to eliminate measurement artefacts due to topographical undulations. The position of the 2D and G peak of each of the probed points on of the unstrained and strained samples are shown in Figure 5c. The mean value of the peak positions in the relative samples show a significant down shift in the signature 2D and G peak at 1585 cm^{-1} and 2685 cm^{-1} respectively. This indicates that the substrate supported graphene is strained by 0.15 ± 0.05%.

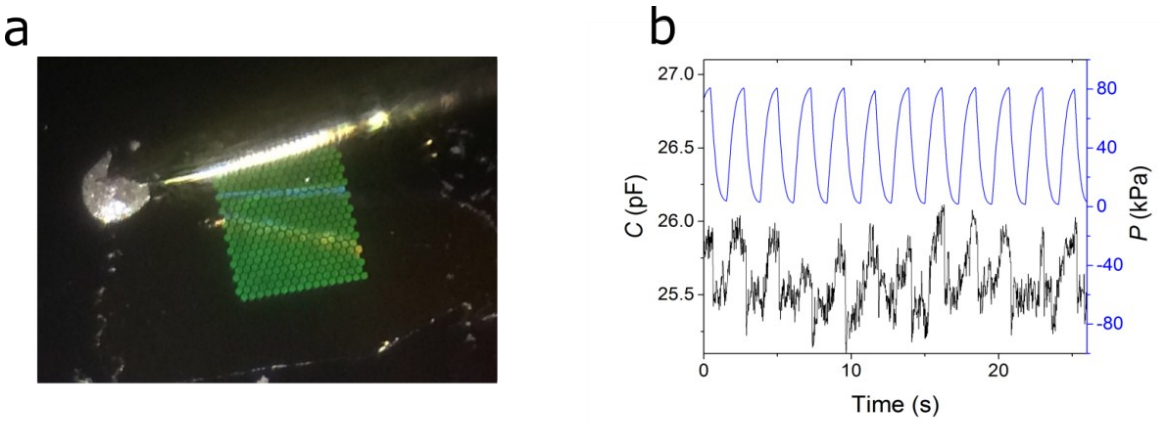

Figure 6 | Sensor characterisation of second generation device. (a) A probe is contacted to the graphene-polymer membrane via a silver epoxy contact at the edge of the transferred film. Scale bar 100 µm. (b) Variation of capacitance over time of a second generation device (black) in reference to the sample chamber pressure.

Supplementary Discussion 6: Pressure testing of high sensitivity design

An optical micrograph of the high sensitivity device electrically contacted with an electrical probe is shown in **Figure 6a**. The pressure-capacitance response of the same device is shown in reference to the pressure inside the test chamber in **Figure 6b**. Despite the large sensitivity of the device, a significant increase in noise (0.2 pF) is measured in comparison to devices with design 1 for model verification (5 fF). We attribute this noise due to charge leakage through the oxide as well as surface charges on the substrate. We support this by further characterisation of the dielectric as discussed in Supplementary Discussion 7.

Supplementary Discussion 7: Characterisation of sensor dielectric

We characterised the dielectric of both generations of devices by conducting C-V sweeps between the top graphene-polymer layer and the silicon substrate. Measurements were taken with an E4990A Network Analyser (Keysight Technologies) at 1 kHz with a sweep rate of 0.15 V/s and a 50 mV AC signal superimposed on a DC voltage bias. Figure 7a shows the capacitance of device design 1 as the voltage between the graphene and the silicon gate electrode is swept between -20 and 20 V in the positive and negative direction. The C-V plot shows a threshold voltage of $V_T = 5.2 = V_{dirac}$ which is offset by the Dirac point of CVD graphene. We also observe a slight hysteresis in the C-V characteristics that is likely due to the time constant associated with charging of the dielectric layer as the particular oxide used in this device was formed by wet oxidation. Further we expect some charge leakage due to trapped states at the base of cavities from the deep reactive ion etching (DRIE) process. In contrast, the C-V characteristics of device design 2, as shown in Figure 7b show a breakdown of the device in the depletion region at a voltage of 5.9 V on positively sweeping the bias from -7.5 to 7.5 V. In addition, the negative sweep shows switching characteristics in the device. We note here that the measured device is likely to contain numerous collapsed membranes, resulting in a very small physical distance between the graphene-polymer film and the silicon gate. Moreover, the sub-cavities etched directly through

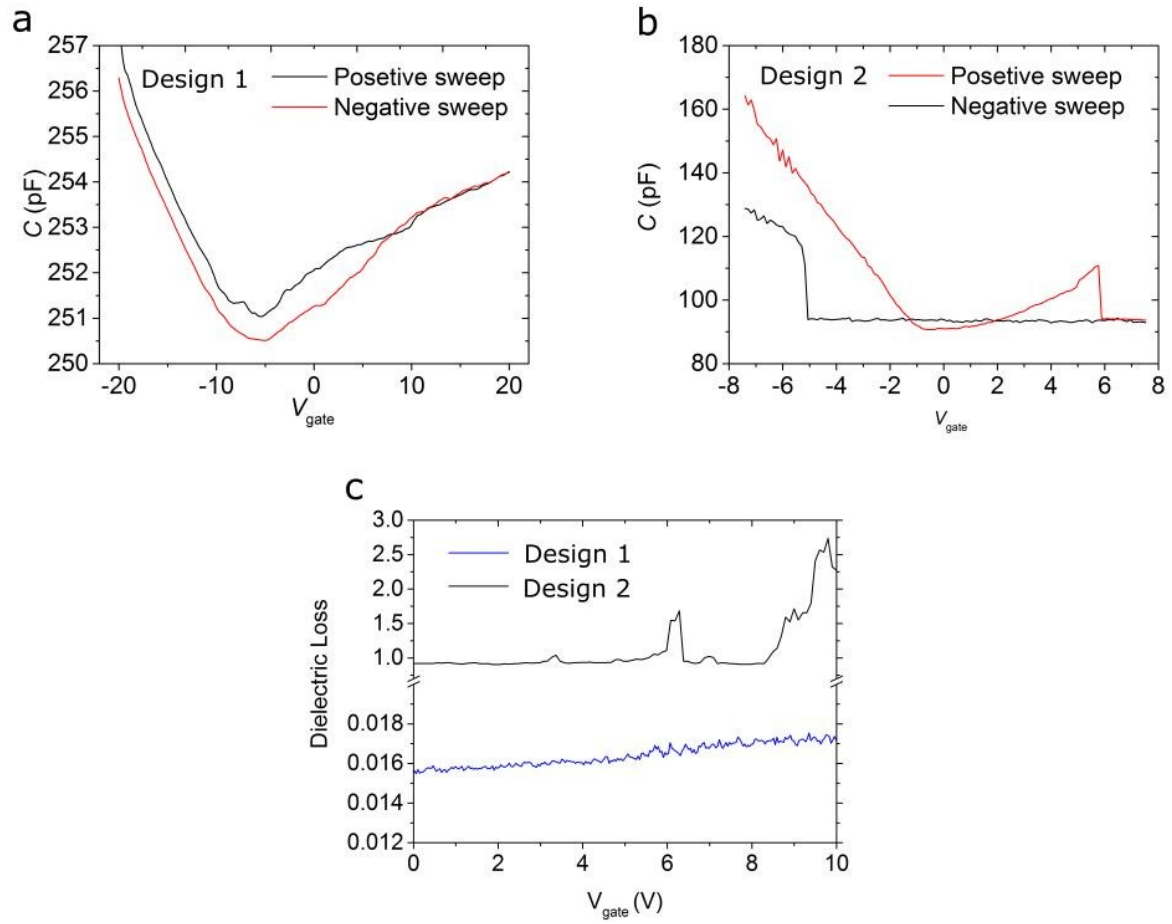

Figure 7 | Sensor characterisation of second generation device. (a) A probe is contacted to the graphene-polymer membrane via a silver epoxy contact at the edge of the transferred film. Scale bar 100 µm. (b) Variation of capacitance over time of a second generation device (black) in reference to the sample chamber pressure.

the silicon oxide layer provide an additional path for surface current leakage. We propose that this switching behaviour is attributed to the deflection of suspended membranes over the sub-cavities, whereby the graphene-polymer membrane latches to the sub-cavity base at a $V_{gate} = 5.9\ V$ and is realised again at a $V_{gate} = -5.2\ V$, however, further experiments are required to confirm this. Figure 7c shows the dielectric loss of both device designs as a function of applied gate bias from 0 V to 10 V. Whilst design 1 shows a relatively low loss of 0.016 at 0 V and minimal increase in loss at increasing gate bias, design 2 shows sharp spikes in loss throughout the positive voltage sweep. This further supports the charge leakage mechanisms described above.

Supplementary references

1. Suk, J. W. *et al.* Transfer of CVD-Grown Monolayer Graphene onto Arbitrary Substrates. *ACS Nano* **5,** 6916–6924 (2011).

2. Dokukin, M. E. & Sokolov, I. Quantitative Mapping of the Elastic Modulus of Soft Materials with HarmoniX and PeakForce QNM AFM Modes. *Langmuir* **28,** 16060–16071 (2012).

3. Koenig, S. P., Boddeti, N. G., Dunn, M. L. & Bunch, J. S. Ultrastrong adhesion of graphene membranes. *Nat. Nanotechnol.* **6,** 543–546 (2011).

4. Bunch, J. S. *et al.* Impermeable Atomic Membranes from Graphene Sheets. *Nano Lett.* **8,** 2458–62 (2008).

5. Cao, Z. *et al.* A blister test for interfacial adhesion of large-scale transferred graphene. *Carbon N. Y.* **69,** 390–400 (2014).